ACS APPLIED MATERIALS & INTERFACES

Research Article

www.acsami.org

Facile Synthesis of Hierarchical Networks Composed of Highly Interconnected V_2O_5 Nanosheets Assembled on Carbon Nanotubes and Their Superior Lithium Storage Properties

Ruixiang Yu,[†,∥] Chaofeng Zhang,[†,‡,§,∥] Qing Meng,[†] Zhixin Chen,[§] Huakun Liu,[†] and Zaiping Guo*[,†,‡,§]

[†]Institute for Superconducting & Electronic Materials, University of Wollongong, Wollongong, New South Wales 2522, Australia

[‡]College of Chemistry and Chemical Engineering, Hubei University, Wuhan, Hubei 430062, China

[§]School of Mechanical, Materials & Mechatronics Engineering, University of Wollongong, Wollongong, New South Wales 2500, Australia

Supporting Information

ABSTRACT: Hierarchical networks with highly interconnected V_2O_5 nanosheets (NSs) anchored on skeletons of carbon nanotubes (CNTs) are prepared by a facile hydrothermal treatment and a following calcination for the first time. Benefiting from these unique structural features, the as-prepared CNT@V_2O_5 material shows dramatically excellent electrochemical performance with remarkable long cyclability (137−116 mA h g^{-1} after 400 cycles) at various high rates (20 C to 30 C) and very good rate capability for highly reversible lithium storage. The excellent electrochemical performance suggests its promising use as a cathode material for future lithium-ion batteries.

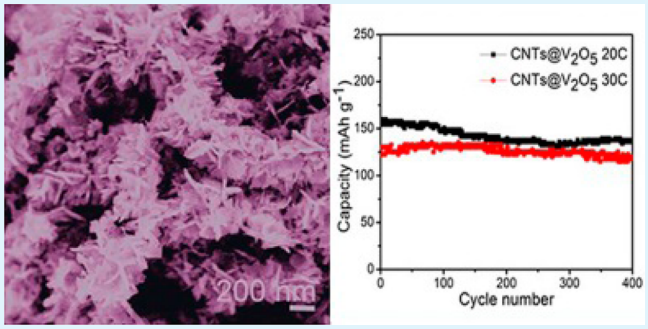

KEYWORDS: *carbon nanotubes, V_2O_5, cathode, lithium ion batteries*

1. INTRODUCTION

Currently, among all the different kinds of rechargeable batteries, lithium-ion batteries (LIBs), which have been attracting enormous interest, would be one of the best choices for powering electric vehicles (EVs) and hybrid electric vehicles (HEVs).[1] Their commercial use in EVs and HEVs, however, is still hindered by their low capacity, safety issues, poor stability, and low rate performance.[2] For further development of LIBs to rise to these serious challenges, substantial efforts have been made to exploit competitive anode and cathode materials. Due to their relatively low capacity compared to anode materials, developing cathode materials with high capacity, high rate capability, and long lifespan is more crucial than it is for anode materials to meet the growing requirements for reducing pollution and greenhouse gas emissions caused by petroleum consumption.[3]

Among the potential cathode materials, orthorhombic vanadium pentoxide (V_2O_5) has attracted great attention since 1976 as a very promising cathode material for next-generation LIBs, due to its low cost and abundant resources, as well as its variety of coordination numbers and oxidation states.[4−7] Specifically, high theoretical capacities of 294 and 442 mA h g^{-1} can be gained with the intercalation of two or three Li^+ ions, respectively.[6,8] Further commercial use of V_2O_5 as cathode for LIBs has been impeded, however, by its structural instability and poor kinetics, including its low electric conductivity and slow Li^+ ion diffusion, resulting in fast capacity fading and low rate capacity.[6,9] To overcome the kinetic problem and stabilize the structure, one strategy is to design nanostructured forms of V_2O_5, for example, hollow/porous structures,[10] one-dimensional (1D) nanobelts/nanorods/nanowires,[8,11−14] and two-dimensional (2D) nanosheets,[15] for the purposes of shortening transport lengths for both electrons and Li^+ ions, enlarging the electrode/electrolyte contact area, and reducing the lattice strain associated with lithium intercalation. Although the electrochemical performance of V_2O_5 has shown great improvement, most of these nanostructures so far have not proved to be very successful in improving the rate capacity and cyclability of V_2O_5 electrodes. Another approach involves combining the active materials with a conductive matrix, thus overcoming the weakness of the poor conductivity.[4,8] For instance, both V_2O_5 nanowires mixed with carbon nanotubes (CNTs) and V_2O_5 loaded among sheets of graphene paper have been reported to demonstrate that the use of conductive materials can enhance the capacity retention of the V_2O_5 and lead to better rate performance due to the improvement in the electronic conductivity.[4,8,16] It can be anticipated that conductive materials could play several positive roles in improving the electrochemical performance of V_2O_5.

Received: August 11, 2013
Accepted: November 15, 2013
Published: November 15, 2013

As a new member of the carbon family, carbon nanotubes, first reported by Iijima in 1991, have generated enormous interest in functional nanomaterials and their various applications.[17,18] Due to the covalent sp^2 bonds between individual carbon atoms, a carbon nanotube shows a tensile strength around a hundred times higher than that of steel and can tolerate huge strains before mechanical failure. CNTs also possess tunable surface properties, well-defined hollow interiors, and a high theoretical electrical conductivity (exceeding 5×10^{-5} S cm^{-1} at room temperature). All their fascinating properties render them very suitable for advanced applications in the areas of electronics, batteries, and capacitors, as well as heterogeneous catalysis.[16,18,19] In the past two decades, CNTs have been used as an attractive material for either anode or cathode in LIBs,[16,20,21] and the encouraging results obtained in these studies are based on the great advantages of CNTs, including high surface area and electrical conductivity. Therefore, it is a very promising strategy to prepare nanosized V_2O_5 with a particular structure on a carbon matrix to achieve LIBs with good cycling performance combined with high rate capacity and long cycle life. In the special structure, the CNT network can work as a highly conductive matrix, which also provides supporting interfaces for anchoring the V_2O_5 nanomaterials.

Here, we first report a facile hydrothermal approach for synthesizing a hierarchical structured V_2O_5 cathode material consisting of CNTs covered by interconnected V_2O_5 nanosheets (denoted as CNTs@V_2O_5). Such CNTs@V_2O_5 integration networks could possibly exhibit synergism of the robust CNTs and the interconnected V_2O_5 nanosheets (V_2O_5–NSs). Specifically, the CNTs and interconnected V_2O_5–NSs could effectively maintain the electrode integrity during charge/discharge processes with the help of the mechanical strength of the CNTs and the high porosity between the V_2O_5–NSs, and facilitate the electronic and ionic transportation. When evaluated as a cathode material for LIBs, the nanocomposite manifests quite remarkable electrochemical performance in terms of cycling stability at high current rate and superior rate capability.

2. EXPERIMENTAL DETAILS

2.1. Materials Synthesis. The CNTs supporting V_2O_5–NSs were prepared by a facile hydrothermal method, as illustrated in Figure 1.

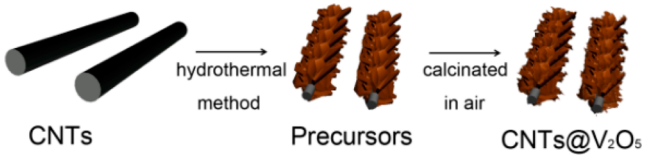

Figure 1. Schematic illustration of the synthesis process for CNTs@V_2O_5.

Typically, acid-treated multiwalled CNTs (7 mg) were dispersed in a mixture of cetyltrimethylammonium bromide (CTAB, 0.3 g) and isopropyl alcohol (IPA, 30 mL) by sonication. Then, 1-methyl-2-pyrrolidinone (MP, 50 μL) and vanadium(V) oxytriisopropoxide (VOT, 200 μL) were injected into the black suspension. After 15 minutes of stirring, the mixture was transferred to a Teflon-lined stainless steel autoclave and heated in an oven at 190°C for 15 h. The product was collected, washed thoroughly by centrifugation with ethanol several times, and dried overnight in a vacuum oven at 60°C. The target product, the CNTs@V_2O_5 nanosheets, was achieved by heating the precursor in a tube furnace at 320°C for 0.5 h with a heating rate of 0.5°C/min. In order to demonstrate the effects of the CNTs, V_2O_5 microflowers (V_2O_5-mf) assembled from V_2O_5–NSs were also prepared by a similar method without CNTs and surfactant in the preparation process.

2.2. Materials Characterization. The products were characterized by X-ray powder diffraction (XRD; GBC MMA diffractometer, Cu Kα, λ = 1.5406 Å). The morphologies and structures were examined by using a field-emission scanning electron microscope (FESEM; JEOL JSM-7500FA) and a transmission electron microscope (TEM; JEOL, 2011). Thermogravimetric analysis (TGA) was conducted at a heating rate of 10°C from room temperature to 800°C under air flow.

2.3. Electrochemical Measurements. The working electrode was prepared by mixing the active material (CNTs@V_2O_5), a conductive agent (carbon black, Super-P-Li), and a binder (polyvinylidene difluoride (PVDF), Sigma-Aldrich) in a weight ratio of 70:20:10 to a homogeneous slurry. After being pasted onto aluminium foil, the prepared working electrodes were dried in a vacuum oven at 120°C over 6 h and were then ready for being assembled into the test cells. The test cells consisted of the active materials as the working electrode, Li foil as the counter and reference electrode, a microporous polypropylene film as the separator, and 1 M $LiPF_6$ in a 1:1 (v/v) mixture of ethylene carbonate (EC) and diethyl carbonate (DEC) as the electrolyte. The test cells were assembled in an Ar-filled glove box (H_2O, O_2 < 0.1 ppm, Mbraun, Unilab). The galvanostatic measurements were conducted in the voltage range of 2.5–4 V or 2–4 V versus Li/Li$^+$ at different constant current densities at room temperature by using a battery cycler (Land CT2001 A). For CNTs@V_2O_5, the specific capacity was calculated based on the mass of V_2O_5.

3. RESULTS AND DISCUSSION

The crystal phase of the V_2O_5 in both the V_2O_5-mf and the CNTs@V_2O_5 samples is confirmed by the XRD patterns, as shown in Figure 2a with the peaks labeled, which demonstrates that all the reflections of the samples are in good agreement with the standard pattern of pure orthorhombic V_2O_5 phase (JCPDS card no. 89-0612).[7] The characteristic diffraction peak of CNTs cannot be clearly observed in the XRD pattern of CNTs@V_2O_5, which can be attributed to the following factors: (1) the (110) crystal plane of V_2O_5 is very close to the (002) plane of CNTs, as shown in the inset of Figure 2a; (2) the relatively low content of CNTs in the composite (from the TGA result); and (3) the CNTs are fully covered by the V_2O_5–NSs. The CNT content and the thermal properties of CNTs@V_2O_5 were characterized by TGA in air, as shown in Figure S2a (Supporting Information). An abrupt weight loss occurs between 400 and 550 °C, indicating the oxidation and decomposition of CNTs in air. Therefore, the mass fraction of CNTs in the CNTs@V_2O_5 sample is about 17 wt %.

The morphology and framework of V_2O_5-mf and CNTs@V_2O_5 were then characterized by field-emission scanning electron microscopy (FESEM) and transmission electron microscopy (TEM). As shown in Figure 2b, the as-prepared precursor has the appearance of a "thorn bush", which is composed of one dimensional "spiny branches" 200–400 nm in diameter, larger than the diameter of the CNTs (shown in Figure S2b, Supporting Information). After calcination in air, flakelike nanosheets of V_2O_5 can be observed, as in Figure 2c, which are highly interconnected and cover the CNT skeleton (the inset of Figure 2c). The interconnected V_2O_5–NSs are in intimate contact with the CNTs, which is favorable for the enhancement of conductivity. In good accordance with the above SEM results, TEM image of CNT@V_2O_5 (Figure 2d) shows that CNTs were surrounded by V_2O_5 nanosheets. As can be seen from Figure 2d and f, the nanosheets are about 10–20

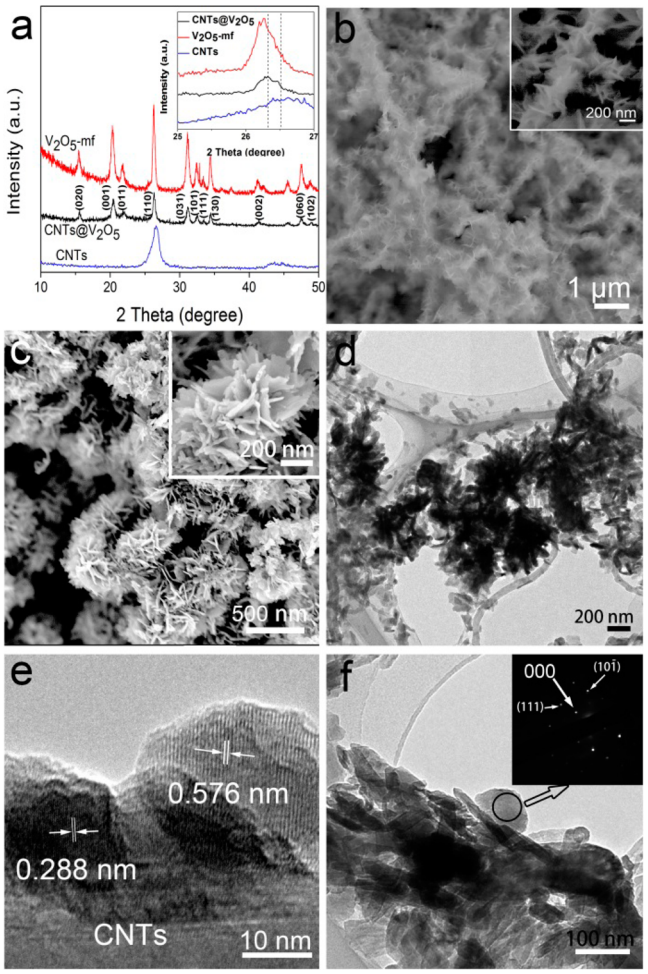

Figure 2. (a) XRD patterns of pure V_2O_5, pure CNTs, and CNTs@V_2O_5. SEM images of (b) precursor of CNTs@V_2O_5 and (c) CNTs@V_2O_5, with inset showing higher magnification. (d) TEM images of CNTs@V_2O_5. (e) The lattice fringe spacing for the selected area. (f) TEM images of CNTs@V_2O_5, the inset shows the corresponding selected area electron diffraction pattern.

nm in thickness and 50−100 nm in diameter. The high resolution TEM image of CNTs@V_2O_5 shown in Figure 2e clearly displays the lattice fringes of V_2O_5. The interlayer spacings of about 0.576 and 0.288 nm, respectively, correspond to the (200) and (301) planes of V_2O_5. The inset of Figure 2f shows the corresponding selected area electron diffraction (SAED) pattern from one nanosheet, which is recorded from the $[1\bar{2}1]$ zone axis which shows the single crystalline nature of the individual V_2O_5 naonsheet. The single crystal structure facilitates the transportation of Li ions.[22] The as-prepared precursor of V_2O_5-mf consists of microflowers with diameter of 1 μm, as shown in Figure S2c (Supporting Information). The inset of Figure S2c (Supporting Information) shows a more highly magnified image of single flower, which is composed of uniform nanosheets. After these flowers were heat treated in air, the as-prepared V_2O_5-mf sample almost maintained the same morphology, as can be observed in Figure S2d (Supporting Information).

We have analysed the intermediates collected at reaction time of 5 and 10 h. After 5 h reaction, only CNTs can be observed from SEM image, indicating the reaction is still at the stage of formation of nanosheets. After reaction for 10 h, there are significant amount of nanosheets formed and surrounded the CNTs, which could be found in the Figure S3 (Supporting Information). Without CTAB in the process, the nanosheets could not be grown on the CNTs, as shown in Figure S4a (Supporting Information). Therefore, surfactant CTAB helps connect nanosheets of hydrophobic V-based organic compound to the hydrophilic hydroxide radical of CNTs, resulting in V-based organic compound nanosheets surrounded CNTs. Figure S4b (Supporting Information) shows the SEM image of precursor fabricated without MP. In the figure, the flowerlike interconnected nanosheets cannot be observed, indicating that MP facilitates the self-assembly of nanosheets. Also, we have tried different chemicals to replace MP in the process, for example, diethylenetriamine and dimethylformamide. As shown in Figure S4c and d (Supporting Information), different sized particles appear, fully proving that MP plays a significant role in forming interconnected nanosheets structure around the CNTs skeleton.

To demonstrate the structural advantages of CNTs@V_2O_5, we have evaluated the electrochemical properties of the two samples as cathode for LIBs. Figure 3a presents representative discharge/charge curves of the CNTs@V_2O_5 sample at 1 C in the voltage window of 2.0−4.0 V. In the first cycle, three plateaus appeared at about 3.3, 3.1, and 2.2 V, which can be attributed to the phase transitions α/ε , ε/δ , and δ/γ , respectively.[23] On the charge curve, three corresponding plateaus related to the Li^+ ion deintercalation process are also observed. The discharge−charge voltage profiles are in good agreement with previous reports.[9,24] The V_2O_5-mf sample gives similar plateaus (Figure 3b), but it exhibits larger irreversible capacity loss over 100 cycles compared with the CNTs@V_2O_5. In detail, the capacity of the V_2O_5-mf electrode drops from 230 to 118 mA h g^{-1} over 100 cycles, while the CNTs@V_2O_5 delivers 285 and 190 mA h g^{-1} at the 1st and the 100th cycle, respectively. The cycling performances of the two samples at the current rate of 1 C are shown in Figure 3c. The CNTs@V_2O_5 electrode shows remarkably improved cycling stability, with a capacity loss of 0.34% per cycle, when compared with the V_2O_5-mf sample with a capacity loss of 0.56% per cycle. For both of these two samples, the coulombic efficiency remains close to 100% during the cycling (Figure 3c), suggesting the excellent reversibility of the electrodes. To further investigate the cycling performance, the two samples were cycled at the current rates of 20 C and 30 C, and the results are shown in Figure 3d. When the current rate is increased to 20 C and 30 C, the capacity of V_2O_5-mf electrode drops rapidly to about 40 mA h g^{-1}, due to its sluggish kinetics. Amazingly, CNTs@V_2O_5 shows excellent electrochemical performance at 20 C and 30 C. Specifically, the capacity slowly drops from 157 to 137 mA h g^{-1} at the current rate of 20 C, and from 127 to 116 mA h g^{-1} at the current rate of 30 C after 400 cycles. Charge-discharge voltage profiles of CNTs@V_2O_5 and V_2O_5-mf at the rate of 20 C are shown in Figure S5 (Supporting Information). It can be found that the plateau of 2.2 V for CNTs@V_2O_5 electrode still exists even after 400 cycles (Figure S5a, Supporting Information); however, the plateau of 2.2 V for the V_2O_5-mf electrode disappears (Figure S5b, Supporting Information). Again, this phenomenon demonstrates the advantage of CNTs in the structure. With a narrower voltage window of 2.5−4 V applied for the two samples, although the capacity is relatively lower, the cycling stability is dramatically improved. Similar phenomena are commonly observed.[9] As shown in Figure S6 (Supporting Information), the CNTs@V_2O_5 sample exhibits excellent electrochemical stability, with high capacities of 105

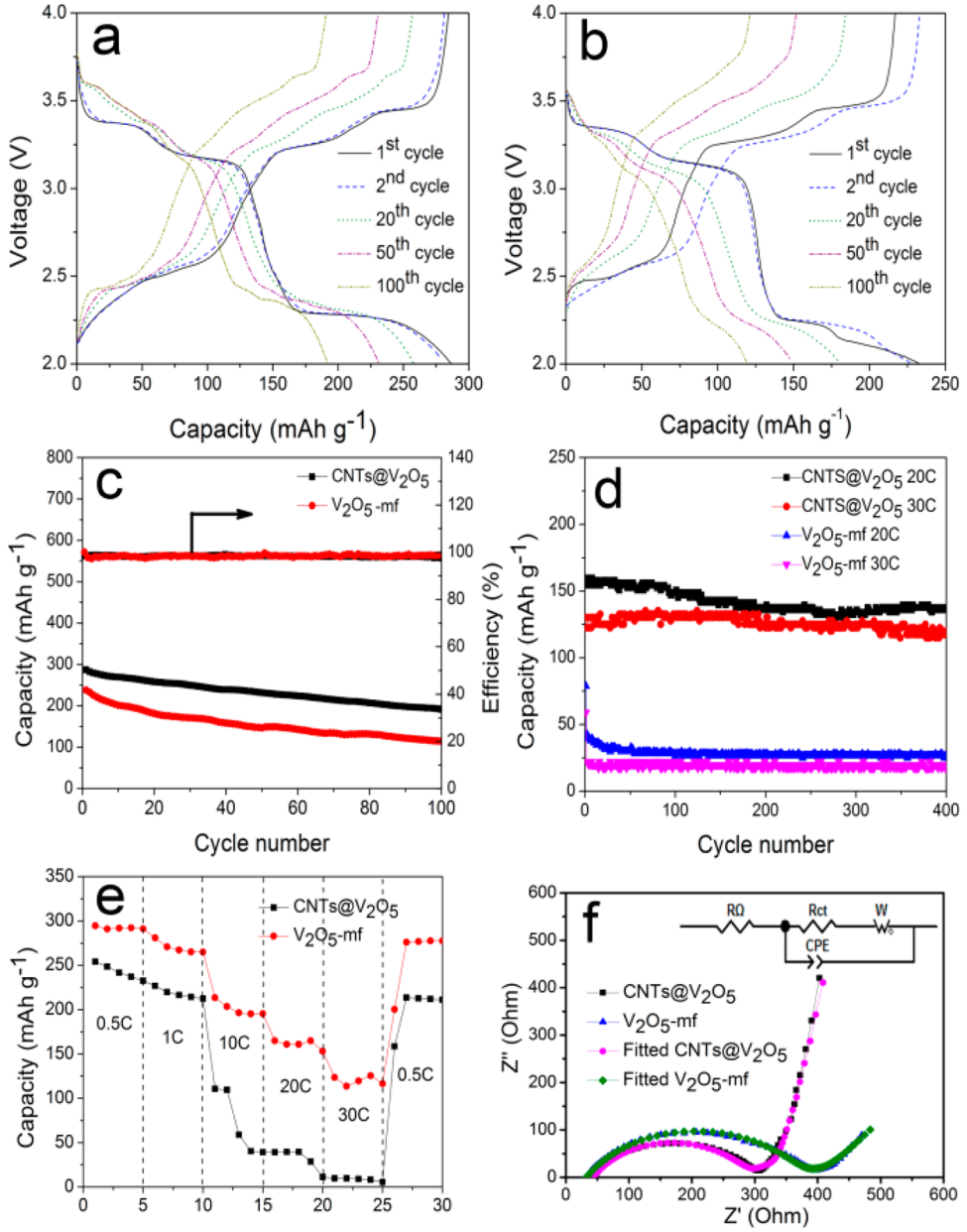

Figure 3. Charge/discharge voltage profiles of CNTs@V_2O_5 (a) and V_2O_5-mf (b) at the current rate of 1 C for the selected cycles indicated. (c) Cycling performance and coulombic efficiency of CNTs@V_2O_5 and V_2O_5-mf in the voltage range of 2.0−4.0 V at the current rate of 1 C. (d) Cycling performance of CNTs@V_2O_5 and V_2O_5-mf in the voltage range of 2.0−4.0 V at the current rates of 20 C and 30 C. (e) Rate capability of CNTs@V_2O_5 and V_2O_5-mf at various current rates. (f) Electrochemical impedance spectra (EIS), fitted EIS curves, and the equivalent circuit (inset) used to fit the impedance data.

and 95 mA h g^{-1} that were retained after 500 cycles at the current rates of 20 C and 30 C (corresponding to capacity loss of 0.025% and 0.031% per cycle), respectively. In contrast, the V_2O_5-mf only delivered specific capacities of about 72 and 30 mA h g^{-1}, with fast fading after 500 cycles, at the current rates of 20 C and 30 C, respectively. Moreover, the rate capability of CNTs@V_2O_5 is also much better than that of V_2O_5-ms, as demonstrated in Figure 3e. The CNTs@V_2O_5 electrode displayed better cycling performance than the V_2O_5-mf at the different current rates. After a deep cycling at 30 C, the CNTs@V_2O_5 electrode can almost regain its initial capacity when the current rate returns back to 0.5 C. For the V_2O_5-mf electrode, in contrast, the capacity is quickly reduced as the current rate increase, down to about 40 mA h g^{-1} at the high current rates of 20 C and 30 C. In order to understand the effects of CNTs in the CNTs@V_2O_5 composite electrode, we then investigated the electrochemical performance of working electrodes directly by mixing CNTs@V_2O_5 and PVDF, with less carbon black (5%) or without carbon black (0%). As observed from Figure S7 (Supporting Information), the capacity of the CNTs@V_2O_5 electrode drops as the content of carbon black decreases. However, the performance of CNTs@V_2O_5 electrode without carbon black is still better than that of V_2O_5-mf electrode containing 20% carbon black. In addition, when the content of carbon black in V_2O_5-mf is increased to 30% (Figure S8) (Supporting Information), the electrochemical performance of V_2O_5-mf is still remarkably worse than that of CNTs@V_2O_5. In summary, the CNTs@

dx.doi.org/10.1021/am4033444 | ACS Appl. Mater. Interfaces 2013, 5, 12394−12399

Table 1. Fitted EIS Results for CNTs@V_2O_5 and V_2O_5-mf Electrodes

	fitted results						
	R_Ω	R_{ct}	W-R	W-T	W-P	CPE-T	CPE-P
CNTs@V_2O_5	43.41	247	125.8	21.32	0.43359	5.2979×10^{-5}	0.67356
V_2O_5-mf	32.84	339.4	111.9	132.5	0.29192	6.145×10^{-5}	0.65367

V_2O_5 electrode exhibits better cycling life and improved rate capability compared to the V_2O_5-mf electrode. The main reason is that the 2D interconnected V_2O_5−NSs and CNTs could provide large specific surface area for more reactive sites and electrode-electrolyte interface, as well as shortening diffusion pathways, enabling easier Li^+/electron transport. In addition, the CNTs in the structure also effectively reduce the polarization when the CNTs@V_2O_5 electrodes were cycled at high current rate. As illustrated in Figure S9 (Supporting Information), the conductive CNTs could effectively accelerate the electron transport for the V_2O_5−NSs.[25] In Figure S9a (Supporting Information), the V_2O_5-mf electrode was composed of relatively large particles (about 1−1.5 μm) with undesirable interparticle resistance, which failed to provide efficient electron transport between active materials and current collector substrate. On the contrary, besides the carbon black, the CNTs in the CNTs@V_2O_5 electrode also could provide sufficient ways for charge transfer; loose structures between the V_2O_5 sheets are beneficial for fast transfer of Li^+ (Figure S9b, Supporting Information). Additionally, the structural robustness of the CNTs is also favorable for the improved electrochemical performance.

To study the effects of the unique structure on the charge transfer, electrochemical impedance spectroscopy (EIS) was performed. Figure 3f shows the Nyquist plots of the V_2O_5-mf and CNTs@V_2O_5 electrodes. In the equivalent circuit (inset), CPE is the constant phase-angle element, involving double layer capacitance; and W is the Warburg impedance, reflecting the solid-state diffusion of Li ions into the bulk of the active materials. R_Ω and R_{ct} represent the ohmic resistance (total resistance of the electrolyte, separator, and electrical contacts) and the charge transfer resistance, respectively. The Nyquist plots that are shown for the two samples are similar, displaying a depressed semicircle in the high-middle frequency region, which could be assigned to the charge transfer resistance (R_{ct}), and an inclined line in the low frequency region, which represents the Warburg impedance. Table 1 displays the fitted results, which shows that the charge-transfer resistance R_{ct} for CNTs@V_2O_5 (about 247 Ω cm^{-2}) is approximately 70% of that for V_2O_5-mf (339.4 Ω cm^{-2}), indicating enhanced charge transfer in the CNTs@V_2O_5 electrode.

4. CONCLUSIONS

We have successfully prepared hierarchically structured networks with interconnected V_2O_5−NSs anchored on skeletons of CNTs by a facile hydrothermal treatment and a following calcination process for the first time. The CNTs and 2D V_2O_5−NSs could work synergistically to provide sufficient tolerance for the volume variation during Li^+ insertion/extraction, accelerate the kinetic process of ion diffusion, and exhibits higher electrical conductivity and structural stability. With the benefits of the above unique characteristics, CNTs@V_2O_5 manifests dramatically improved electrochemical performance in terms of long cyclability at high rate and very good rate capability when they are used as cathode material for LIBs. The obtained results suggest that this is a good direction to improve the electrochemical performance of electrode materials for high power LIBs.

■ ASSOCIATED CONTENT

Supporting Information

XRD of the precursor, TGA, addition SEM images of V_2O_5-mf, SEM images of precursors synthesized at different conditions, and details of electrochemical results. This material is available free of charge via the Internet at http://pubs.acs.org.

■ AUTHOR INFORMATION

Corresponding Author

*Telephone: 61-2-42215225. E-mail: zguo@uow.edu.au.

Author Contributions

‖R.Y. and C.Z. contributed equally. The manuscript was written through contributions of all authors. All authors have given approval to the final version of the manuscript.

Notes

The authors declare no competing financial interest.

■ ACKNOWLEDGMENTS

Financial support provided by the Australian Research Council (ARC) through an ARC Discovery project (DP1094261) is gratefully acknowledged. The authors would also like to thank the Electron Microscopy Centre (EMC) at the University of Wollongong for the electron microscopy characterization.

■ REFERENCES

(1) Goodenough, J. B.; Kim, Y. *Chem. Mater.* **2010**, *22*, 587−603.
(2) Wang, S. Q.; Li, S. R.; Sun, Y.; Feng, X. Y.; Chen, C. H. *Energy Environ. Sci.* **2011**, *4*, 2854−2857.
(3) Hosono, E.; Kudo, T.; Honma, I.; Matsuda, H.; Zhou, H. S. *Nano Lett.* **2009**, *9*, 1045−1051.
(4) Seng, K. H.; Liu, J.; Guo, Z. P.; Chen, Z. X.; Jia, D. Z.; Liu, H. K. *Electrochem. Commun.* **2011**, *13*, 383−386.
(5) Whittingham, M. S. *J. Electrochem. Soc.* **1976**, *123*, 315−320.
(6) Wang, Y.; Cao, G. Z. *Chem. Mater.* **2006**, *18*, 2787−2804.
(7) Zhang, C.; Chen, Z.; Guo, Z.; Lou, X. W. *Energy Environ. Sci.* **2013**, *6*, 974−978.
(8) Liu, H. M.; Yang, W. S. *Energy Environ. Sci.* **2011**, *4*, 4000−4008.
(9) Pan, A. Q.; Wu, H. B.; Zhang, L.; Lou, X. W. *Energy Environ. Sci.* **2013**, *6*, 1476−1479.
(10) Rui, X.; Zhu, J.; Sim, D.; Xu, C.; Zeng, Y.; Hng, H. H.; Lim, T. M.; Yan, Q. *Nanoscale* **2011**, *3*, 4752−4758.
(11) Mai, L. Q.; Xu, X.; Xu, L.; Han, C. H.; Luo, Y. Z. *J. Mater. Res.* **2011**, *26*, 2175−2185.
(12) Wang, Y.; Zhang, H. J.; Lim, W. X.; Lin, J. Y.; Wong, C. C. *J. Mater. Chem.* **2011**, *21*, 2362−2368.
(13) Cheah, Y. L.; Aravindan, V.; Madhavi, S. *ACS Appl. Mater. Interfaces* **2012**, *4*, 3270−3277.
(14) Perera, S. D.; Patel, B.; Bonso, J.; Grunewald, M.; Ferraris, J. P.; Balkus, K. J. *ACS Appl. Mater. Interfaces* **2011**, *3*, 4512−4517.
(15) Liu, Y.; Uchaker, E.; Zhou, N.; Li, J.; Zhang, Q.; Cao, G. *J. Mater. Chem.* **2012**, *22*, 24439−24445.
(16) Chen, X. Y.; Zhu, H. L.; Chen, Y. C.; Shang, Y. Y.; Cao, A. Y.; Hu, L. B.; Rubloff, G. W. *ACS Nano* **2012**, *6*, 7948−7955.
(17) Iijima, S. *Nature* **1991**, *354*, 56−58.

(18) Zhang, Q.; Huang, J.-Q.; Qian, W.-Z.; Zhang, Y.-Y.; Wei, F. *Small* **2013**, *9*, 1237−1265.
(19) Heister, E.; Neves, V.; Lamprecht, C.; Silva, S. R. P.; Coley, H. M.; McFadden, J. *Carbon* **2012**, *50*, 622−632.
(20) Wu, H. B.; Lou, X. W.; Hng, H. H. *Chem.—Eur. J.* **2012**, *18*, 3132−3135.
(21) Toprakci, O.; Toprakci, H. A. K.; Ji, L.; Xu, G.; Lin, Z.; Zhang, X. *ACS Appl. Mater. Interfaces* **2012**, *4*, 1273−1280.
(22) Zhang, C. F.; Feng, C. Q.; Zhang, P.; Guo, Z. P.; Chen, Z. X.; Li, S.; Liu, H. K. *RSC Adv.* **2012**, *2*, 1643−1649.
(23) Delmas, C.; Cognac-Auradou, H.; Cocciantelli, J. M.; Ménétrier, M.; Doumerc, J. P. *Solid State Ionics* **1994**, *69*, 257−264.
(24) Li, Y.; Yao, J.; Uchaker, E.; Yang, J.; Huang, Y.; Zhang, M.; Cao, G. *Adv. Energy Mater.* **2013**, *3*, 1171−1175.
(25) Wang, Y.; Wang, Y.; Hosono, E.; Wang, K.; Zhou, H. *Angew. Chem., Int. Ed.* **2008**, *47*, 7461−7465.